

Portland State University

PDXScholar

Mechanical and Materials Engineering Faculty
Publications and Presentations

Mechanical and Materials Engineering

10-21-2022

Visualization of Cathode Spot Control using Laser irradiation and oxide addition in wire arc additive manufacturing of titanium alloys

Tae Hyun Lee

Korea Institute of Industrial Technology, Incheon

Cheolhee Kim

Portland State University, cheol@pdx.edu

Je Hoon Oh

Hanyang University

Dong Hyuck Kam

Korea Institute of Industrial Technology, Incheon

Follow this and additional works at: https://pdxscholar.library.pdx.edu/mengin_fac



Part of the [Mechanical Engineering Commons](#)

Let us know how access to this document benefits you.

Citation Details

Published as: Lee, T. H., Kim, C., Oh, J. H., & Kam, D. H. (2022). Visualization of cathode spot control using laser irradiation and oxide addition in wire arc additive manufacturing of titanium alloys. *Journal of Laser Applications*, 34(4), 042024.

This Post-Print is brought to you for free and open access. It has been accepted for inclusion in Mechanical and Materials Engineering Faculty Publications and Presentations by an authorized administrator of PDXScholar. Please contact us if we can make this document more accessible: pdxscholar@pdx.edu.

VISUALIZATION OF CATHODE SPOT CONTROL USING LASER IRRADIATION AND OXIDE ADDITION IN WIRE ARC ADDITIVE MANUFACTURING OF TITANIUM ALLOYS

Paper #188

Tae Hyun Lee^{1,2}, Cheolhee Kim^{1,3*}, Je Hoon Oh², Dong Hyuck Kam^{1,*}

¹ Joining R&D Group, Korea Institute of Industrial Technology, Incheon 21999, South Korea

² Department of Mechanical Design Engineering, Hanyang University, Seoul 04763, South Korea

³ Department of Mechanical and Materials Engineering, Portland State University, OR 97207, USA

* Contact: kamdong@kitech.re.kr; chkim@pdx.edu, chkim@kitech.re.kr

Abstract

Arc instability is one of the most critical problems in gas-metal-arc (GMA) based wire arc additive manufacturing (WAAM) of titanium (Ti) alloys. It can result in a poor bead surface, surface oxidation, and spattering. In particular, the relocation of the cathode spot area is the main cause of big spatters because of the high thermal energy of the molten droplet at the molten pool surface. In this study, two cathode spot control techniques were applied using auxiliary laser heating and pre-laid oxides, and the behaviors of the cathode spots and arc were visualized using high-speed photography. When the laser beam was irradiated in front of the GMA, a cathode spot was formed at the laser irradiation position, and the cathode jet did not interfere with the arc plasma and droplet transfer from the GMA. However, when the distance between the GMA and the laser irradiation position increased by more than 8 mm, multiple cathode spots were established, and spattering increased. The pre-laid Ti oxide particles increased the metal deposition efficiency by establishing multiple and dispersed cathode spots rather than a concentrated cathode spot by droplet impingement. It was found that the volumetric transfer efficiencies (excluding spattering) for the laser-assisted control and Ti oxide powder were up to 99.87% and 91.2%, respectively.

Introduction

Titanium (Ti) and its alloys have excellent material properties, such as a high strength-to-weight ratio and fatigue strength, good corrosion and high-temperature creep resistance, and biocompatibility. However, because there are downsides to using Ti alloys in traditional manufacturing processes of forming, welding, and machining, the application of Ti alloys has been limited to dedicated industries because of their high material and manufacturing costs [1].

Additive manufacturing (AM) can realize near-net-shape forming without traditional forming and minimize material removal after forming. With the recent advances in AM processes, various applications have been introduced in aerospace [2,3], oil and gas [4], power plant [5], and biomedical [6-8] industries.

AM processes for the fabrication of Ti alloys can be classified into powder bed fusion (PBF), powder-based direct energy deposition (DED), and wire-based DED. Among them, wire-based DED processes have the best deposition efficiency and are suitable for AM of large-scale products. An electric arc, electron beam, or laser beam are utilized as a power source in wire-based DED processes. Wire-arc AM (WAAM) has the advantages of higher deposition rate and process flexibility compared with wire-electron beam and wire-laser beam processes [9-11]. The gas metal arc (GMA) process is a representative arc process for WAAM [9]. During GMA-based WAAM, an electric arc is coaxially generated from the consumable electrode wire, which enables an easy tool path design and a high heat efficiency of up to 85% [12].

In order to establish an electric arc, electrons are emitted from the negative electrode (cathode) and transferred to the positive electrode (anode). There are two electron emission mechanisms in WAAM: thermionic and non-thermionic, and the thermionic emission mechanism works on Ti alloy cathodes [13,14]. In GMA-based WAAM, the consumable wire is the anode, and the substrate is the cathode. The consumable wire is melted by the arc heat, and molten droplets are transferred into the liquid pool on the substrate. The impinging droplets on the molten pool have a higher temperature than the molten pool because they are heated through the arc column [14,15].

In thermionic emission, electrons are emitted at the location with the maximum temperature by the thermionic mechanism, so that the cathode spot is formed at the droplet impinging location on the liquid pool. Electrode emission at the cathode generates a jet

flow called a cathode jet. The cathode jet in Ti WAAM can eject droplets out of the liquid pool of the substrate, interfere with droplet transfer into the pool, and deteriorate arc plasma stability.

To avoid arc and droplet transfer instability, auxiliary laser heating has previously been suggested. According to Shinn et al. [16], when a Nd:YAG laser beam was irradiated at the leading edge of the molten pool, the laser could stabilize arc cathode spots. Pardal et al. [17] applied laser stabilization to a low-heat input GMA process called cold-metal-transfer (CMT). However, arc and droplet behavior according to various laser parameters have not been fully explained and discussed in these previous studies.

In the GMA process, the surface oxide on the molten pool plays an important role in non-thermionic emission. The surface oxide lowers the work function and causes a tunneling effect and arc switching [13]. By adding O₂ or CO₂ to the shielding gas, oxide is formed along the molten pool boundary, which facilitates non-thermionic emission on the bead side and mitigates undercut formation [18-20]. Because Ti alloys have strong oxygen affinity [21], pure inert gas is supplied as a shielding gas in WAAM. The effect of oxide on the cathode phenomenon has not been previously examined.

In this study, arc and droplet phenomena was investigated in the GMA-WAAM process of a Ti-6Al-4V alloy. Laser irradiation and oxide pre-laying were selected as cathode spot control methods. By employing two high-speed cameras, arc and drop transfer were simultaneously recorded. The effects of laser power and laser-arc distance was quantitatively discussed and the effect of pre-laying oxide was also clearly visualized.

Experimental setup

Ti-6Al-4V plates with a thickness of 5 mm were used as substrates, and an equivalent solid wire (AWS ER Ti-5) with a diameter of 1.2 mm was used as a deposition wire. The chemical compositions of the substrate and the wire are given in Table 1.

The deposition wire was fed into the substrate through a deposition torch, and electric power was applied in the constant voltage mode by an WAAM power source. The deposition torch was manipulated by a 6-axis articulated robot at a constant speed during deposition. The torch angle was perpendicular to the substrate, and 99.9% purity argon gas was supplied through the deposition torch as a shielding gas (Fig 1). The details of the WAAM parameters are listed in Table 2.

An Yb:YAG disk laser with a wavelength of 1030 nm and a maximum output power of 4 kW was used as the laser heating power source. The laser beam with a diameter of 0.6 mm was irradiated on the substrate with an angle of 60 degrees. The distance between the laser and wire aiming was defined as an offset distance (Fig. 2). The offset and laser power were varied in the experiment. The details of the laser heating parameters are listed in Table 3.

Table 1. Chemical compositions of Ti-6Al-4V substrate and electrode wire

Substrate: Ti-6Al-4V							Unit: wt%
Ti	Al	V	C	Fe	N	O	
89.0	6.36	3.95	0.011	0.18	0.011	0.01	
Wire: ER Ti-5							Unit: wt%
Ti	Al	V	C	Fe	N	O	
89.4	6.20	3.95	0.008	0.15	0.001	0.13	

Table 2. WAAM process parameters

WFR ¹ (m/min)	Arc current (A)	Arc voltage (V)	Travel speed (m/min)	GFR ² (L/min)	CTWD ³ (mm)
9.3	200	27	0.6	20	15

¹ Wire feed rate; ² Gas flow rate; ³ Contact tip-to-workpiece distance

Table 3. Laser heating process parameters

Beam diameter (mm)	Laser angle (deg)	Offset (mm)	Laser power (W)
0.6	60	2, 4, 6, 8	500, 1000, 1500, 2000

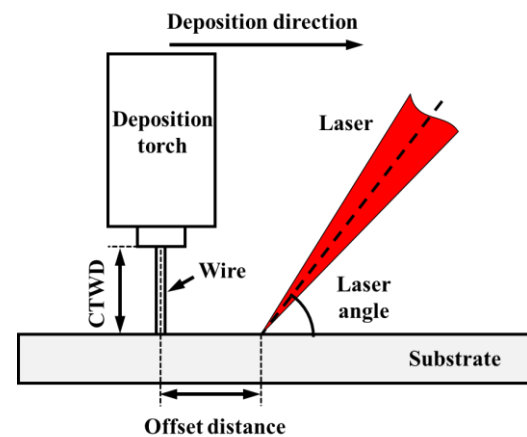


Fig. 1 Schematic diagram of torch and laser beam arrangement

In the oxide pre-laying test, 99.9% purity Ti oxide powder with a maximum diameter of 44 μm was overlaid on the substrate prior to deposition (Fig. 2). The width and thickness of the pre-lay were 20 mm and 0.3 mm, respectively.

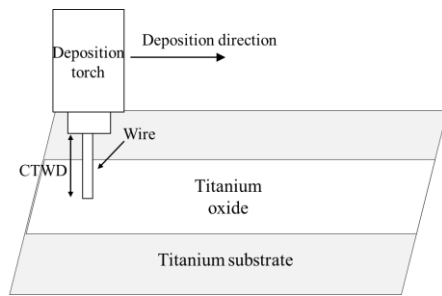


Fig. 2 Ti oxide pre-laying test

Arc and wire melting behaviors were visualized using two high-speed cameras: monochrome and color (Fig. 3). The two cameras were synchronized, and the sampling rate was 5,000 frames per second. A diode laser beam with a wavelength of 808 nm and power of 120 W was used as the illumination for the high-speed photography. The illumination beam had a diameter of 30 mm on the substrate. An 808-nm bandpass filter with a full-width half maximum of 3 nm was used in the monochrome imaging. A 1/500 neutral density filter was adopted in the color imaging.

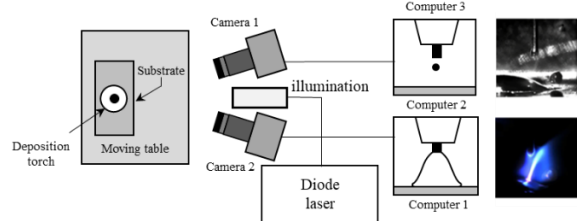


Fig. 3 Schematic of high-speed photography

Since spattering is a convenient index to quantify process stabilization, the ratio of spattering to droplet transfer was defined as the spattering ratio. During spattering, when a droplet comes in contact with the molten pool, it is partially ejected out of the pool, and the remaining droplet is transferred into the pool. The volume of spatters was calculated from high-speed images under the assumption that it was spherical. The ratio of the transferred volume to the original droplet volume was defined as a volumetric transfer rate. The spattering ratio and volumetric transfer rate were calculated from high-speed images over 1.0 s.

Results and discussion

Deposit stabilization by laser irradiation

In the GMA-WAAM of the Ti alloys, the width and location of the deposit were nonuniform and the surface quality was deteriorated because of spatters adhering to the surface (Fig. 4). Molten droplets from the wire electrode were transferred into the substrate through the downward arc plasma flow. When a droplet contacted the molten pool surface, a strong repelling plasma flow, a cathode jet, was established,

and the droplet was rebounded out of the molten pool (Fig. 5). From high-speed imaging, it was confirmed that spattering occurred with an 89.5% probability when a droplet was transferred into the pool and only 90.3% in volume was transferred into the deposit. The authors of this study have visualized the behaviors of the droplet, arc plasma, and molten pool during titanium WAAM in their recent publication [15]. The transferred droplet elevates the temperature at the point of contact so that it becomes higher than that of the present cathode spot location, and the cathode spot location moves to the droplet-molten surface contact point. The cathode spot movement was accompanied by a strong cathode jet, which pushed the droplet back out of the molten pool. In addition, arc wandering caused by the cathode spot movement resulted in an inconsistent deposit geometry.



Fig. 4 Bead appearance in GMA-WAAM of Ti-6Al-4V alloy

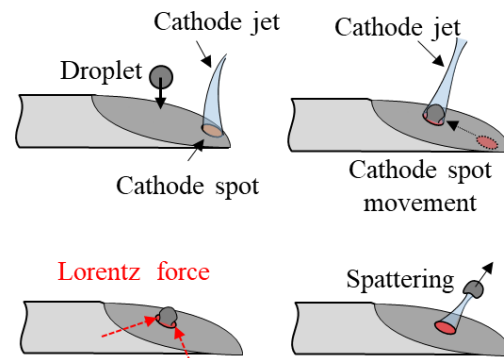


Fig. 5 Spatter generation mechanism in Ti GMA-WAAM

As demonstrated by Shinn et al. [16] and Pardal et al. [17], laser irradiation in front of the arc heat source stabilized the droplet transfer and deposit width in WAAM, but the process parameters of laser power and offset distance affected the degree of stabilization (Fig. 6). The surface quality was distinctly improved when the laser power was 1,000 W or higher. In particular, when the offset distance was 4 mm or higher, severe spatter adhesion was observed at a laser power of 500 W. When the offset distance was 8 mm, more spatter was generated compared with other offset distances. In the configuration of this study, a laser power between 1,000–2,000 W and an offset distance of 2–6 mm are recommended. The behavior of the cathode spot and droplet transfer were analyzed using high-speed photography and are discussed in subsequent sections.

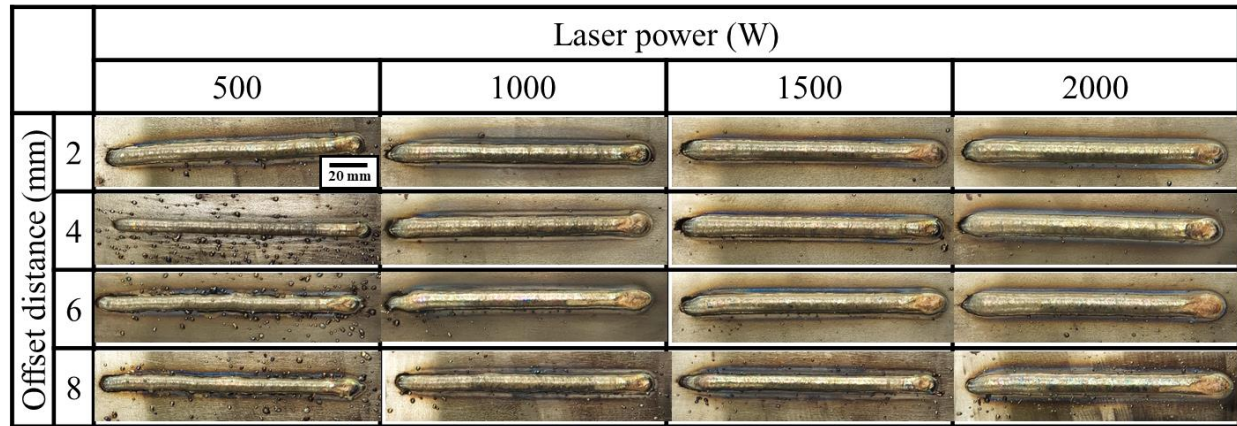


Fig. 6 Effects of the offset distance and laser power on spatter generation

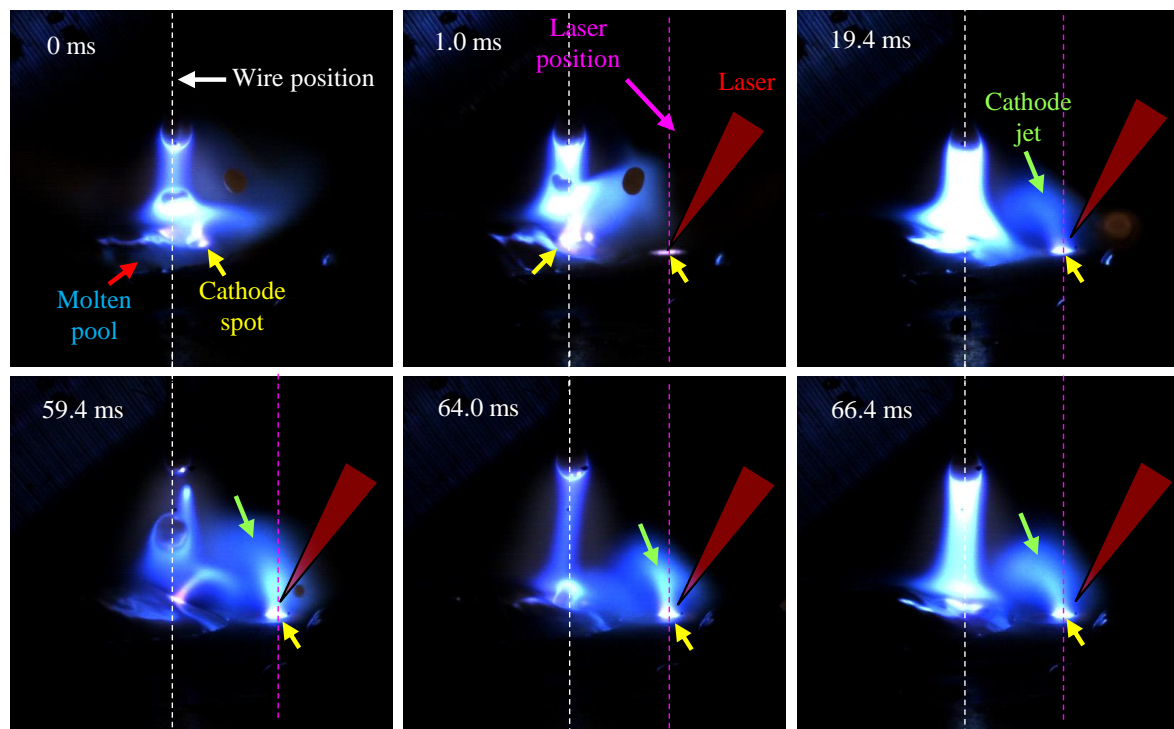


Fig. 7 Stabilization of the cathode spot location by laser irradiation (laser power: 1,500 W, offset: 6 mm)

When the laser was focused on the surface of the molten pool with an appropriate intensity, the laser irradiation raised the local temperature at the focal point higher than that at the droplet transfer location, and the cathode jet was consistently emitted from the laser focal point without intermittent relocation to the droplet transfer location. In Fig. 7, the laser was not irradiated in the first image, and the cathode jet was emitted from the droplet impinging location; spattering was observed in the first and second images. The laser was turned on in the second image, and the primary cathode spot moved to the laser focal point, as seen in the third image. Although a droplet was impinged into the molten pool in the fourth and laser images, the primary cathode spot location was maintained at the laser focal point without movement

toward the droplet impinging location. A relatively weak cathode jet was formed at the droplet impinging location but did not interfere with the droplet transfer.

Effect of offset distance

The increase in laser offset distance reduced the stability of the cathode spot, and the spatter generation was proportional to the offset distance, except in the 500 W laser power cases (Fig. 8). In particular, at a laser power of 1,500 W, the spattering frequency increased by 2.3 times by increasing the offset distance from 2 mm to 8 mm. When the offset distance was 4 mm or less, a cathode spot at the laser focal point was dominant. By increasing the offset distance to 6 mm or higher, an additional cathode jet

emitted from the droplet impinging location was intensified, and three evenly spaced cathode spots were observed at an offset distance of 8 mm (Fig. 9). The increase in the offset distance decreased the difference in brightness of the cathode jet at the laser focal point and the droplet impinging location. At a laser power of 500 W, the cathode spot was observed at the laser focal point only in the 2 mm offset case and at the droplet impinging location in the higher offset cases (Fig. 10).

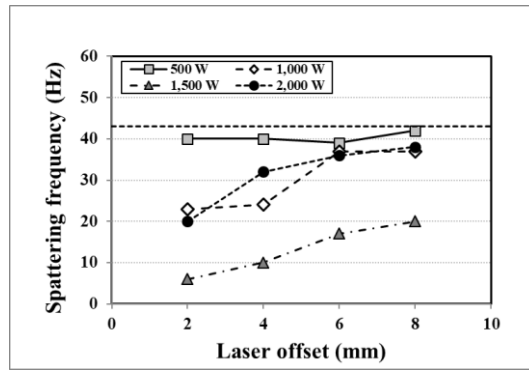


Fig. 8. Effect of laser offset on spatter generation

From the Ti alloy, electrons were emitted by the thermionic cathode emission mechanism. The current density J in thermionic cathode emission can be expressed by the following Richardson–Dushman equation [13]:

$$J = AT^2 \exp\left(-\frac{e\phi}{kT}\right), \quad (1)$$

where A is the Richardson constant, T is the temperature, e is the charge of an electron, ϕ is the

thermionic work function of the cathode surface, and k is the Boltzmann's constant.

The increase in the offset distance decreased the local temperature at the laser focal point, which was determined by superposition of arc plasma heating and laser heating [22]. Therefore, when the temperature difference between the laser focal point and the droplet impinging location was decreased, cathode jet emission formed at the droplet impinging location was increased.

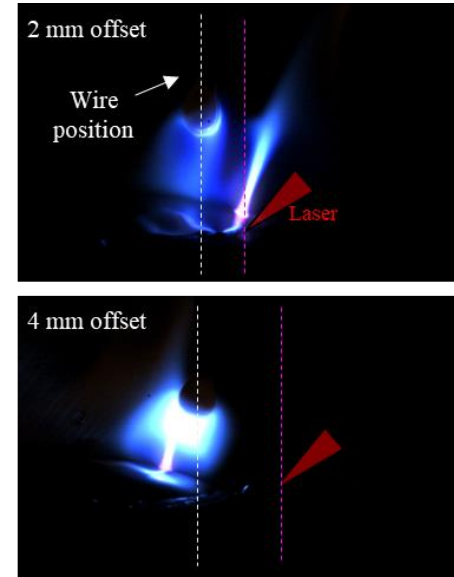


Fig. 10 Cathode jet behavior according to the laser offset at a laser power of 500 W

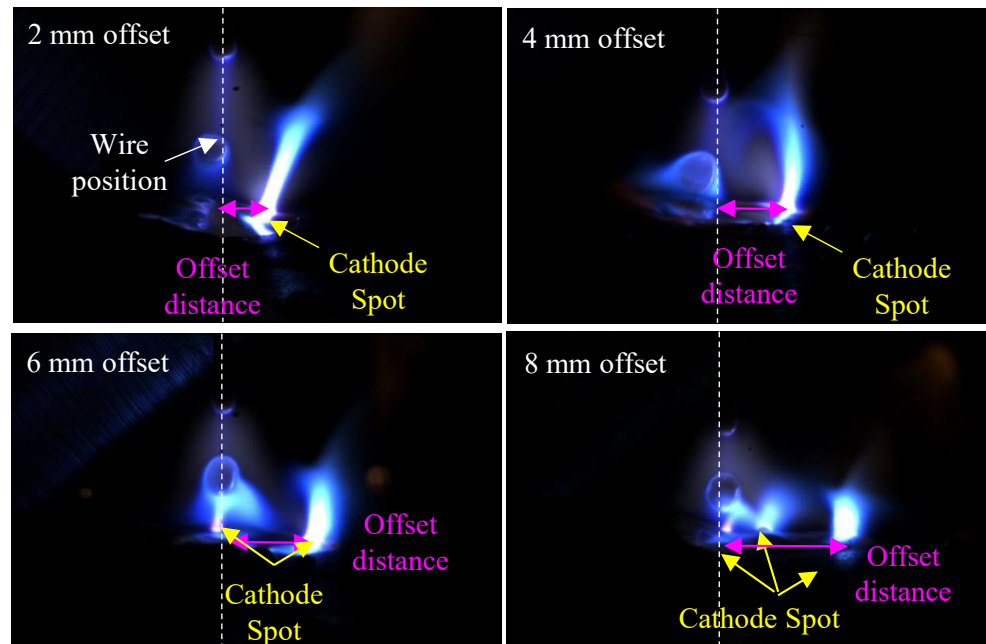


Fig. 9. Cathode jet behavior according to the laser offset at a laser power of 1,500 W

Effect of laser power

Spatter generation decreased with an increase in laser power but increased again at a laser power of 2,000 W (Fig. 11). The mechanism is similar to that in the laser offset cases except for the 2,000 W laser power cases. The increase in laser power increased the local temperature at the laser focal point, which increased the cathode jet from the laser focal point and reduced the spatters caused by the cathode jet from the droplet impinging location.

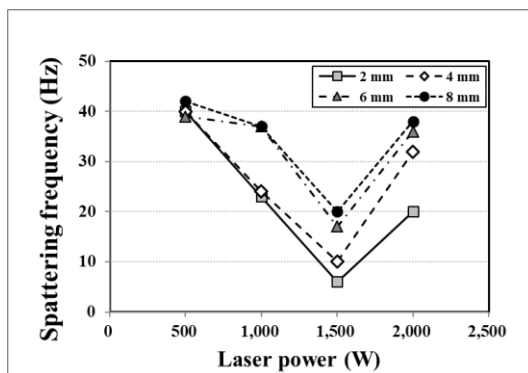


Fig. 11 Effect of laser power on spatter generation. The number of spatters was counted during a 1.0 s interval.

When the laser power was 2,000 W, laser induced plasma was generated and combined with the arc plasma (Fig. 12). Laser-induced plasma could be distinguished from the cathode jet from the laser focal point because it had a relatively weak directionality. Because the laser induced plasma heated a wide area of the molten pool and superheated the droplets, the temperature and cathode jet were increased at the droplet impinging location, and subsequently, more spatters were generated.

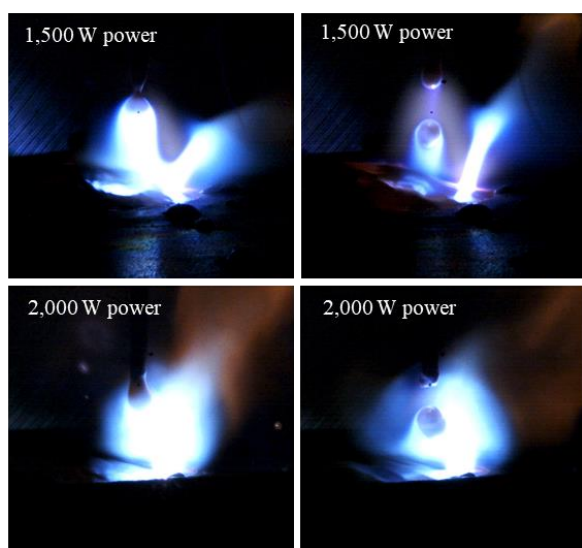


Fig. 12 Cathode jet and plasma behavior according to the laser power at an offset distance of 2 mm

Droplet behavior

The diameter of the free-flight droplets and spattering frequency were measured from high-speed images (Fig. 13). The droplet diameter was inversely proportional to the droplet frequency and showed a similar tendency with the spattering frequency. When the cathode jet was emitted from the droplet impinging location, the upward cathode jet interfered with droplet detachment from the end of the wire, as shown in Fig. 10. Gravity, electro-magnetic force, and surface tension are related to droplet detachment [13,23]; thus, if the upward cathode jet is applied to the hanging droplet at the wire end, more gravity will be required to detach the droplet.

The overall stability and efficiency of the deposit were evaluated using the spattering ratio and volumetric transfer rate. As expected, Figs. 11 and 13b show that the spattering ratio was minimized at a laser power of 1,500 W and decreased by reducing the offset distance (Fig. 14a). The minimum spattering ratio was confirmed as 10.5% at a laser power of 1,500 W and an offset of 2 mm. Compared to the spattering ratio, the volumetric transfer ratio was relatively high, from 89.8% to 99.87%. Similar to the spattering ratio, the volumetric transfer rate was maximized at a laser power of 1,500 W, and the maximum value was 99.87% at a laser power of 1,500 W and an offset of 2 mm.

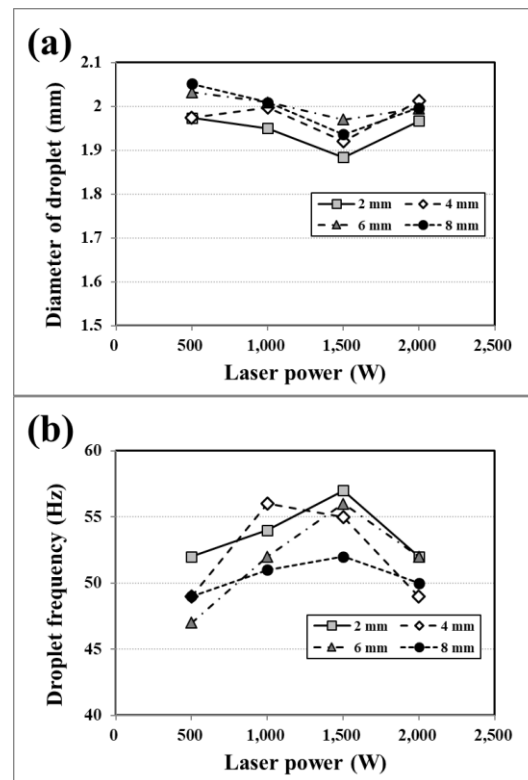


Fig. 13 Measured (a) diameter and (b) frequency of free flight droplet

This is the author's peer reviewed, accepted manuscript. However, the online version of record will be different from this version once it has been copyedited and typeset.
PLEASE CITE THIS ARTICLE AS DOI: 10.2351/17.0000738

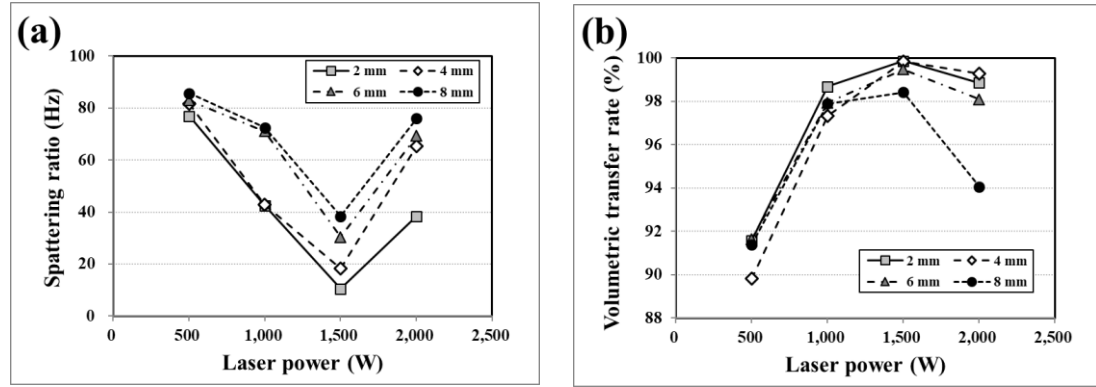


Fig. 14 Calculated (a) spattering ratio and (b) volumetric transfer rate

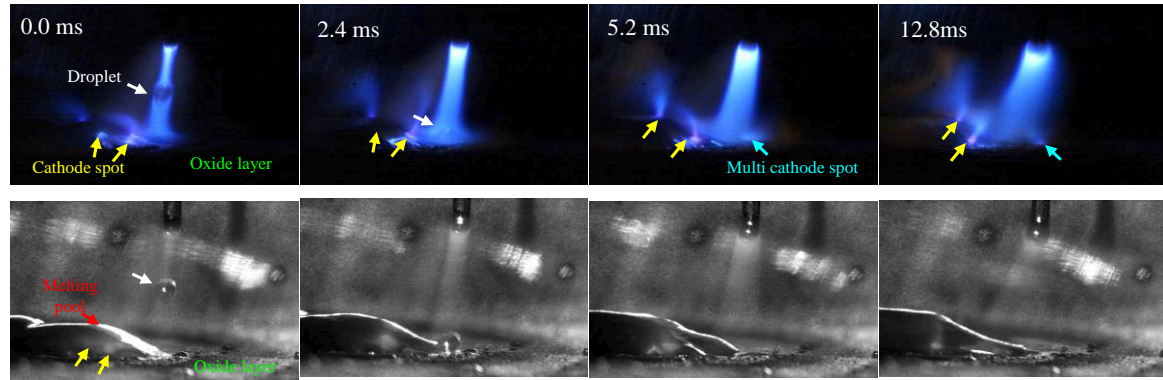


Fig. 15 Cathode spot behavior in oxide prelaying test

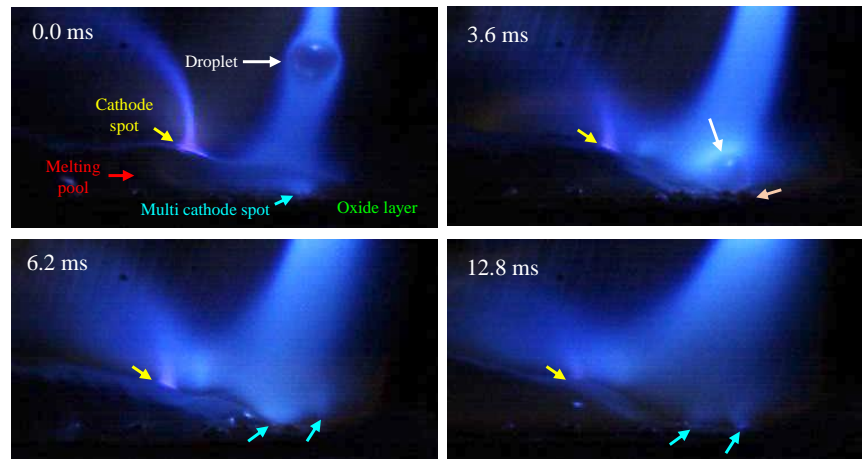


Fig. 16 Multiple cathode spots from oxides

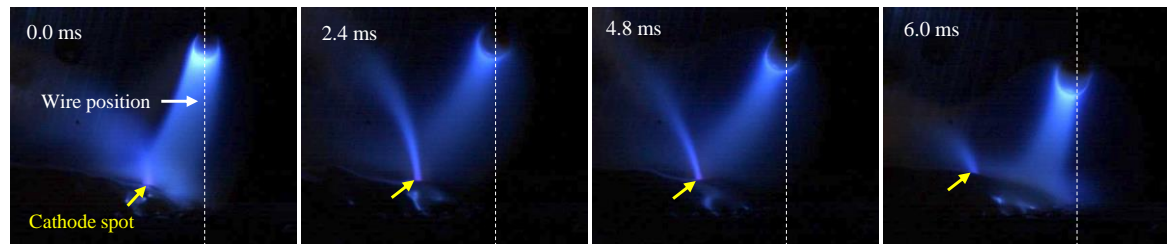


Fig. 17 Arc wandering in the oxide prelaying test

Deposit stabilization by oxide prelaying

Cathode spot control was confirmed in the oxide prelaying test (Fig. 15). The oxide has a relative low work function compared with the Ti alloy, and cathode spots were established from oxides floating on the molten pool although their temperature was lower than that of the droplet impinging location. Multiple cathodes were simultaneously observed on the oxides on the molten pool (Fig. 16). However, oxide prelaying could not completely eliminate arc wandering (Fig. 17), and only 76.2% of droplets were fully transferred into the molten pool; the volumetric transfer rate was 91.2%. Although the oxide prelaying method showed feasibility, more efficiency is necessary for prospective applications.

Conclusions

We examined and visualized the cathode spot and droplet transfer behavior according to laser irradiation and oxide prelaying in Ti GMA-WAAM, and the following conclusions were derived.

- (1) Laser irradiation and oxide prelaying can increase the stability of deposition. The deposit shape was homogenized, and arc wandering was mitigated. Volumetric transfer rates of 89.8% to 99.87% by laser irradiation and 91.2% by oxide prelaying were achieved.
- (2) Laser power and the laser offset distance influenced the cathode spot behavior. The performance was enhanced by increasing the temperature difference between the laser focal point and the droplet impinging location.
- (3) A high laser power and low laser offset raised the local temperature at the laser focal point. However, laser induced plasma was generated by excessive laser power, and a laser power of 1,500 W was recommended in this configuration.
- (4) For the oxide prelaying test, multiple cathode spots were established from floating oxides on the molten pool. An intense cathode spot because of the impinging droplet was simultaneously generated, and the mitigation of arc wandering was limited.

GMA-WAAM of Ti alloys has excellent flexibility and deposition efficiency, and furthermore, its deposit quality can be enhanced by adopting the methods proposed in this investigation.

Acknowledgments

We acknowledge the financial support provided by the Korea Institute of Industrial Technology (Grant No.: EO-22-0005).

References

- [1] ASM International (1992) ASM handbook, 10th ed., Vol. 2: Properties and selection: nonferrous alloys and special-purpose materials, ASM International.
- [2] Uhlmann, E., Kersting, R., Klein, T. B., Cruz, M. F. & Borille, A. V. (2015) Additive manufacturing of titanium alloy for aircraft components, *Procedia CIRP* 35, 55-60.
- [3] Liu, Z., He, B., Lyu, T. & Zou, Y. (2021) A Review on Additive manufacturing of titanium alloys for aerospace applications: directed energy deposition and beyond Ti-6Al-4V, *Journal of the Minerals Metals and Materials Society* 73(6), 1804-1818.
- [4] Sireesha, M., Lee, J., Kranthi Kiran, A. S., Babu, V. J., Kee, B. B. T. & Ramakrishna, S. (2018) A review on additive manufacturing and its way into the oil and gas industry, *RSC Advances* 8(40), 22460-22468.
- [5] Arie, M. A., Shooshtari, A. H. & Ohadi, M. M. (2018) Experimental characterization of an additively manufactured heat exchanger for dry cooling of power plants, *Applied Thermal Engineering* 129, 187-198.
- [6] Hao, Y.-L., Li, S.-J. & Yang, R. (2016) Biomedical titanium alloys and their additive manufacturing, *Rare metals* 35(9), 661-671.
- [7] Trevisan, F., Calignano, F., Aversa, A., Marchese, G., Lombardi, M., Biamino, S., Ugués, D. & Manfredi, D. (2018) Additive manufacturing of titanium alloys in the biomedical field: processes, properties and applications, *Journal of Applied Biomaterials & Functional Materials* 16(2), 57-67.
- [8] Jang, T. S., Kim, D., Han, G., Yoon, C. B. & Jung, H. D. (2020) Powder based additive manufacturing for biomedical application of titanium and its alloys: a review, *Biomedical Engineering Letters* 10(4), 505-516.
- [9] Williams, S. W., Martina, F., Addison, A. C., Ding, J., Pardal, G. & Colegrove, P. (2016) Wire + arc additive manufacturing, *Materials Science and Technology* 32(7), 641-647.
- [10] Lin, Z., Song, K. & Yu, X. (2021) A review on wire and arc additive manufacturing of titanium alloy, *Journal of Manufacturing Processes* 70, 24-45.
- [11] Norrish, J., Polden, J. & Richardson, I. (2021) A review of wire arc additive manufacturing: development, principles, process physics, implementation and current status, *Journal of Physics D: Applied Physics* 54(47), 473001.

This is the author's peer reviewed, accepted manuscript. However, the online version of record will be different from this version once it has been copyedited and typeset.
PLEASE CITE THIS ARTICLE AS DOI: 10.2351/7.0000738

- [12] DuPont, J. & Marder, A. (1995) Thermal efficiency of arc welding processes, *Welding Journal* 74(12), 406s-416s.
- [13] Lancaster, J. (1986) *The Physics of Welding: International Institute of Welding*, 2nd ed., Elsevier.
- [14] Eickhoff, S. T. & Eagar, T. W. (1990) Characterization of spatter in low-current GMAW of titanium alloy plate, *Welding Journal* 69(10), 382s-388s.
- [15] Lee, T. H., Kam, D. H., Oh, J. H. & Kim, C. (2022) Ti-6Al-4V alloy deposition characteristics at electrode-negative polarity in the cold metal transfer-gas metal arc process, *Journal of Materials Research and Technology* 19, 685-696.
- [16] Shinn, B. W., Farson, D. F. & Denney, P. E. (2005) Laser stabilisation of arc cathode spots in titanium welding, *Science and Technology of Welding and Joining* 10(4), 475-481.
- [17] Pardal, G., Martina, F. & Williams, S. (2019) Laser stabilization of GMAW additive manufacturing of Ti-6Al-4V components, *Journal of Materials Processing Technology* 272, 1-8.
- [18] Chae, H. B., Kim, C. H., Kim, J. H. & Rhee, S. H. (2007) Welding phenomena in hybrid laser-rotating arc welding process, *Materials Science Forum* 539-543, 4093-4098.
- [19] Chae, H., Kim, C., Kim, J. & Rhee, S. (2008) The effect of shielding gas composition in CO₂ laser-gas metal arc hybrid welding, *Proceedings of the Institution of Mechanical Engineers, Part B: Journal of Engineering Manufacture* 222(11), 1315-1324.
- [20] Nakamura, T., Hiraoka, K. & Zenitani, S. (2013) Improvement of MIG welding stability in pure Ar shielding gas using small amount of oxygen and coaxial hybrid solid wire, *Science and Technology of Welding and Joining* 13(1), 25-32.
- [21] Lee, Y., Cheon, J. & Kim, C. (2022) Review on Vacuum Laser Beam Welding, *Journal of Welding and Joining* 40(1), 74-83.
- [22] Kim, C., Chae, H., Kim, J. K. & Kim, J. (2007) Optimization of laser-arc interspacing distance during CO₂ laser-GMA hybrid welding by using high-speed imaging, *Advanced Materials Research* 26, 481-484.
- [23] Kim, Y. & Eagar, T. (1993) Analysis of metal transfer in gas metal arc welding, *Welding Journal*, 269s-278s.

This is the author's peer reviewed, accepted manuscript. However, the online version of record will be different from this version once it has been copyedited and typeset.
PLEASE CITE THIS ARTICLE AS DOI: 10.2351/17.0000738

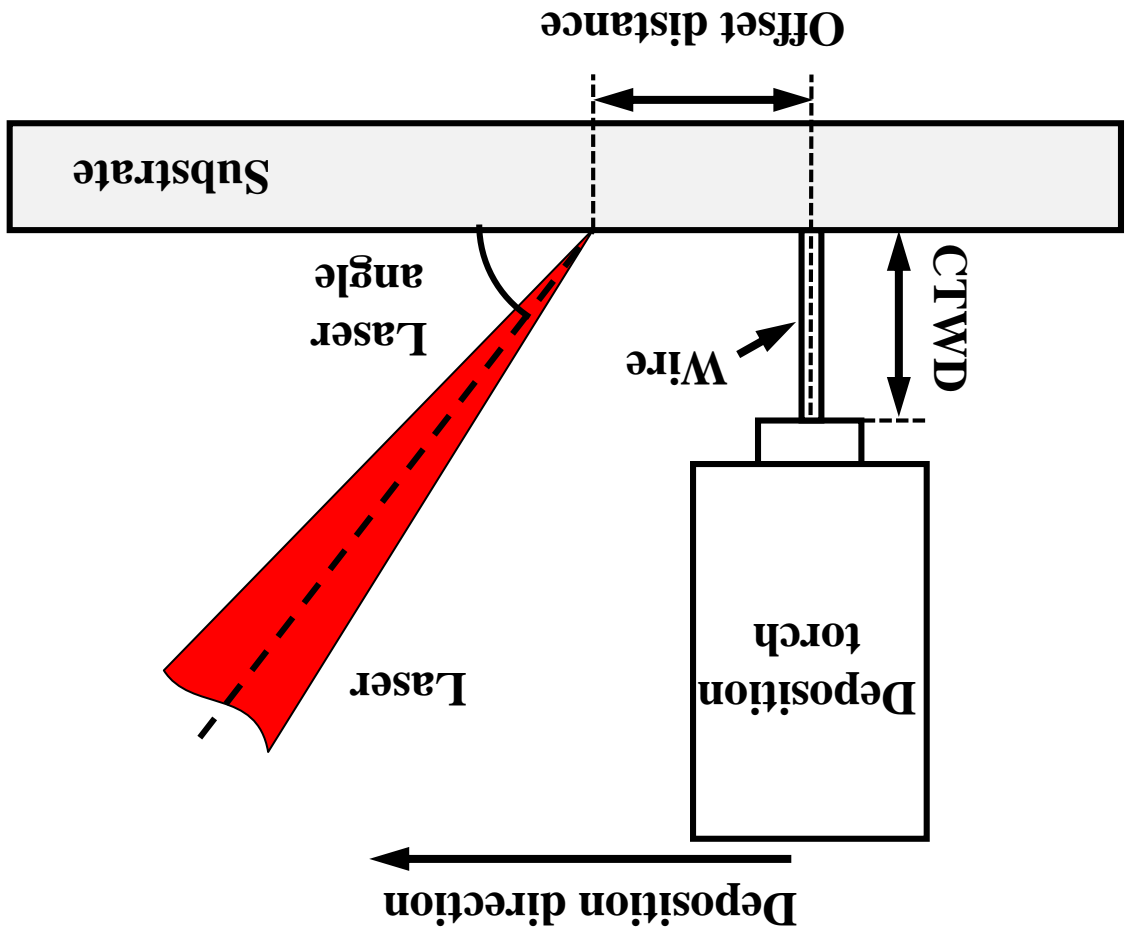


Fig. 1 Schematic diagram of torch and laser beam arrangement

This is the author's peer reviewed, accepted manuscript. However, the online version of record will be different from this version once it has been copyedited and typeset.
PLEASE CITE THIS ARTICLE AS DOI: 10.2351/17.0000738

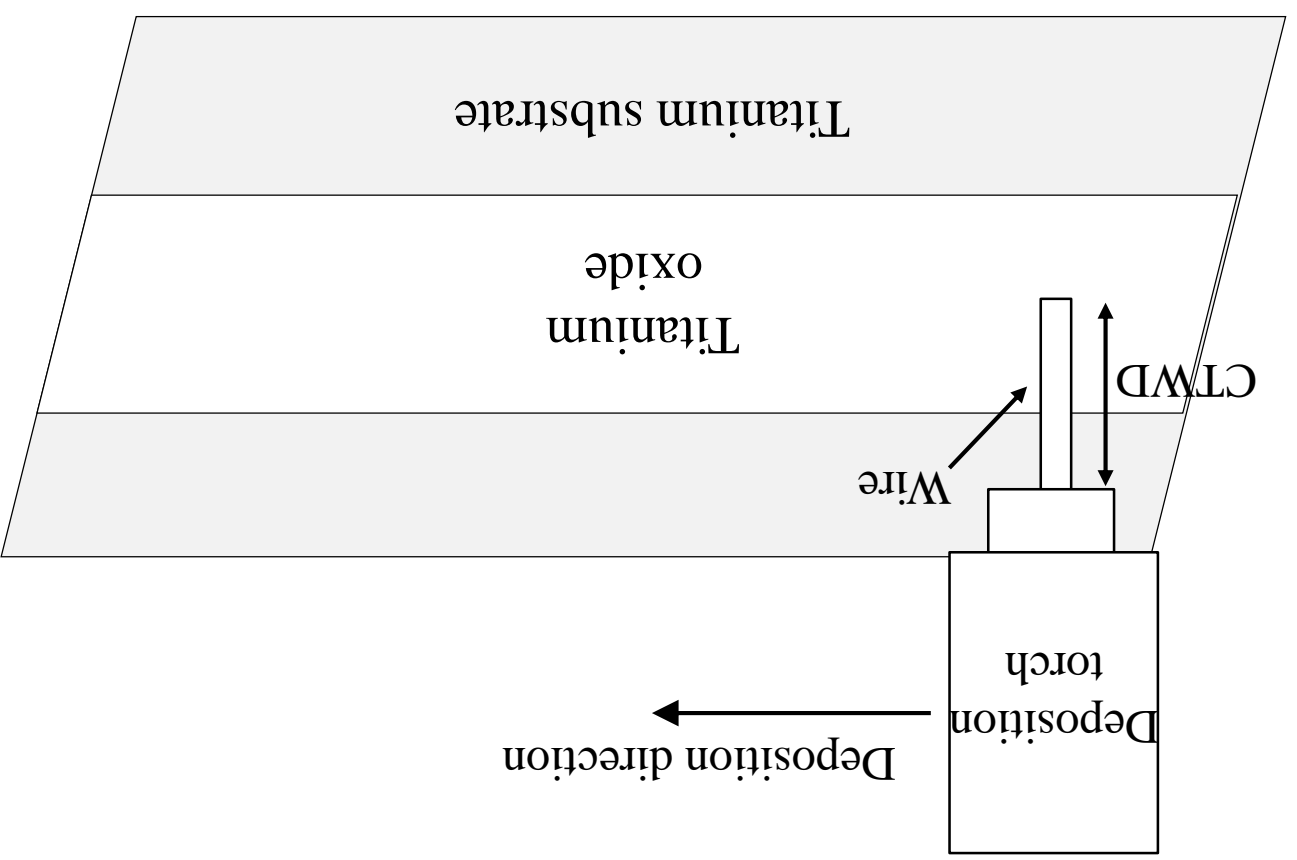


Fig. 2 Ti oxide pre-laying test

This is the author's peer reviewed, accepted manuscript. However, the online version of record will be different from this version once it has been copyedited and typeset.
PLEASE CITE THIS ARTICLE AS DOI: 10.2351/7.0000738

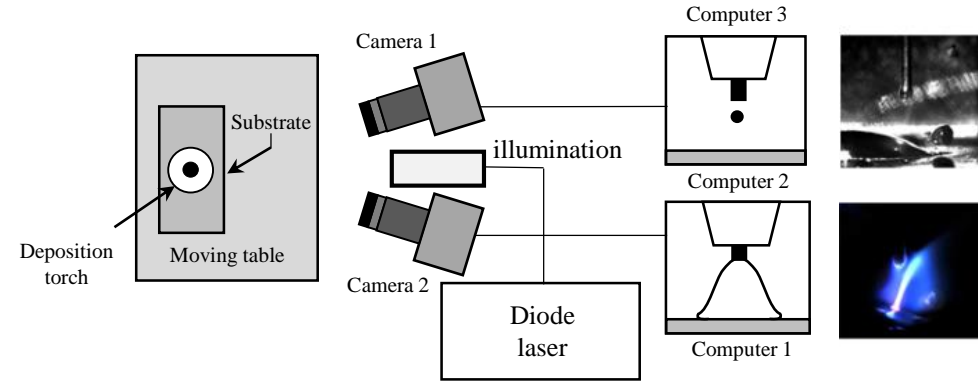


Fig. 3 Schematic of high-speed photography

This is the author's peer reviewed, accepted manuscript. However, the online version of record will be different from this version once it has been copyedited and typeset.

PLEASE CITE THIS ARTICLE AS DOI: 10.2351/17.0000738



Fig. 4 Bead appearance in GMA-WAAM of Ti-6Al-4V alloy

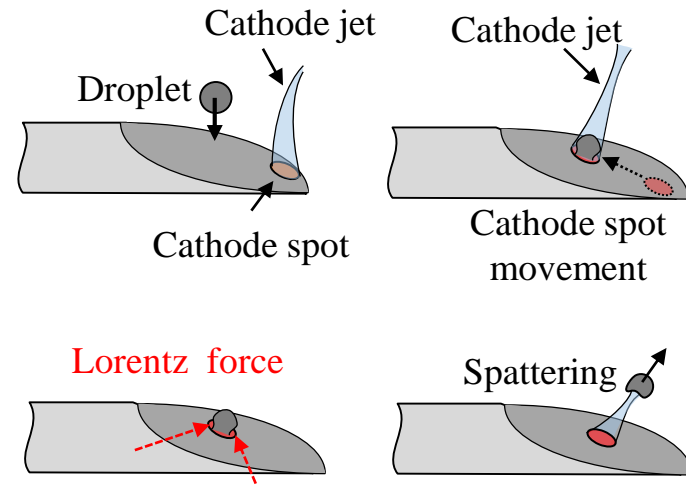


Fig. 5 Spatter generation mechanism in Ti GMA-WAAM

This is the author's peer reviewed, accepted manuscript. However, the online version of record will be different from this version once it has been copyedited and typeset.
PLEASE CITE THIS ARTICLE AS DOI: 10.2351/7.0000738

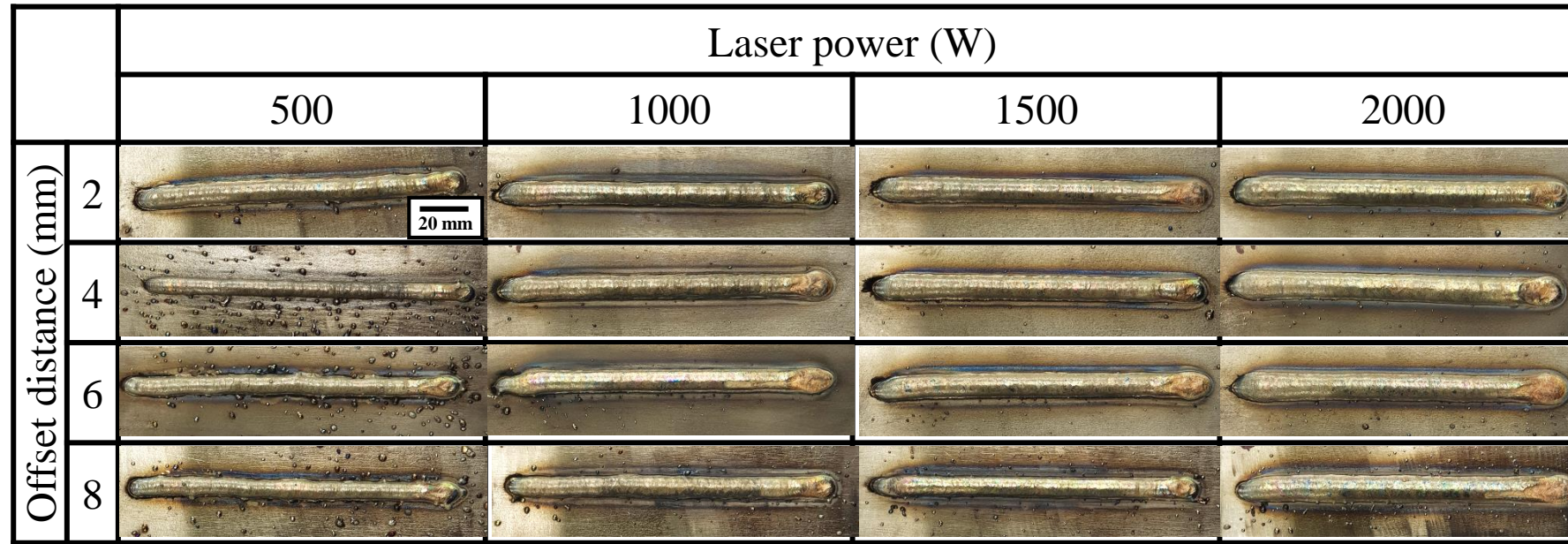


Fig. 6 Effects of the offset distance and laser power on spatter generation

This is the author's peer reviewed, accepted manuscript. However, the online version of record will be different from this version once it has been copyedited and typeset.
PLEASE CITE THIS ARTICLE AS DOI: 10.2351/1.5000738

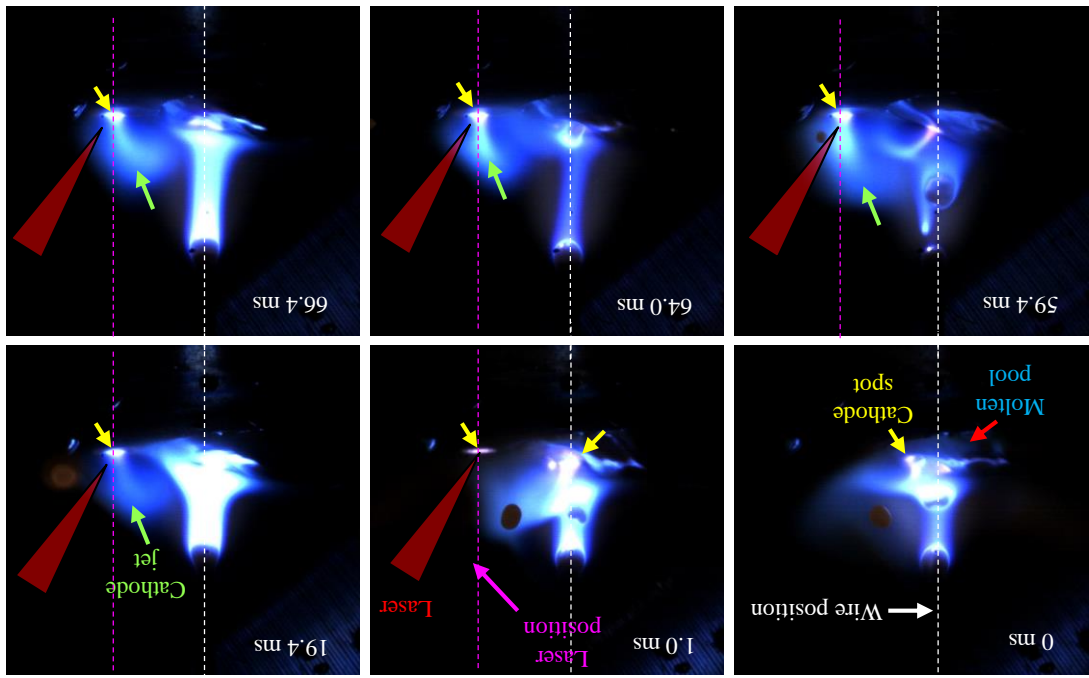


Fig. 7 Stabilization of the cathode spot location by laser irradiation (laser power: 1,500 W, offset: 6 mm)

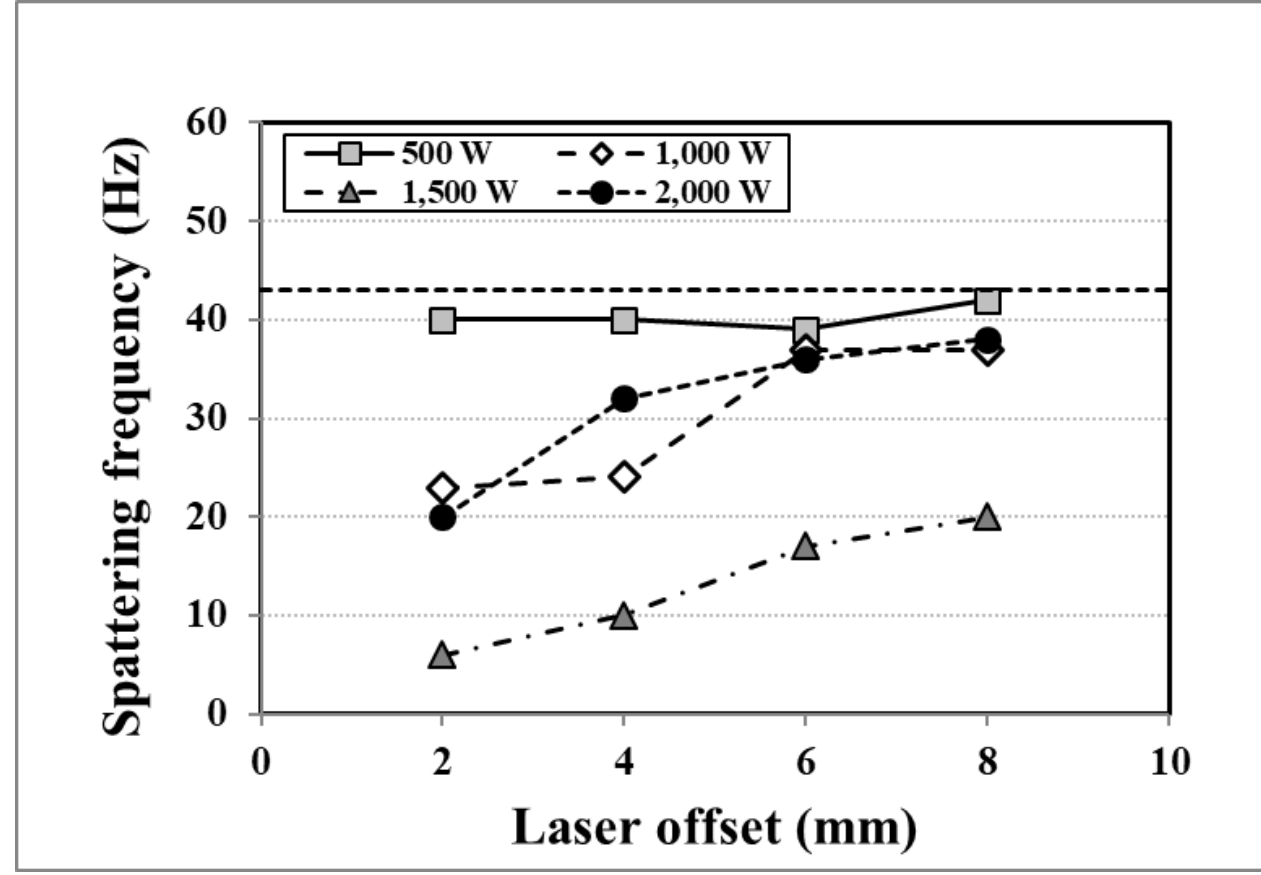


Fig. 8. Effect of laser offset on spatter generation

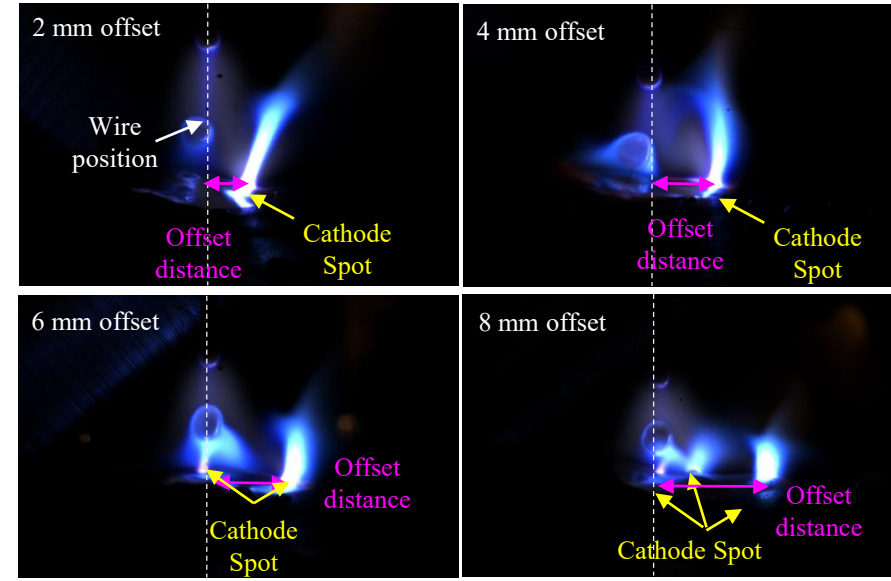


Fig. 9. Cathode jet behavior according to the laser offset at a laser power of 1,500 W

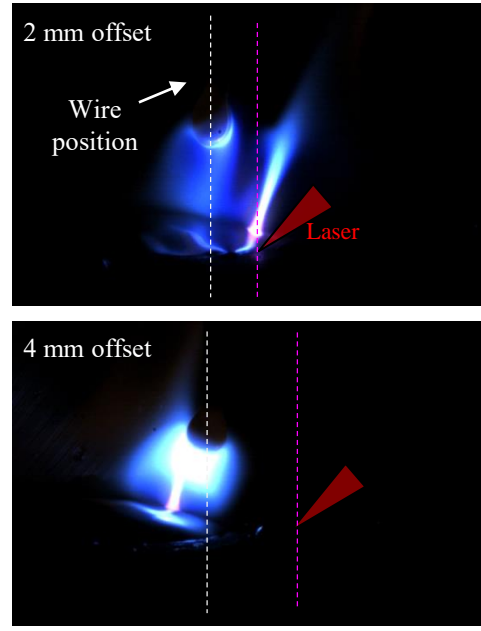


Fig. 10 Cathode jet behavior according to the laser offset at a laser power of 500 W

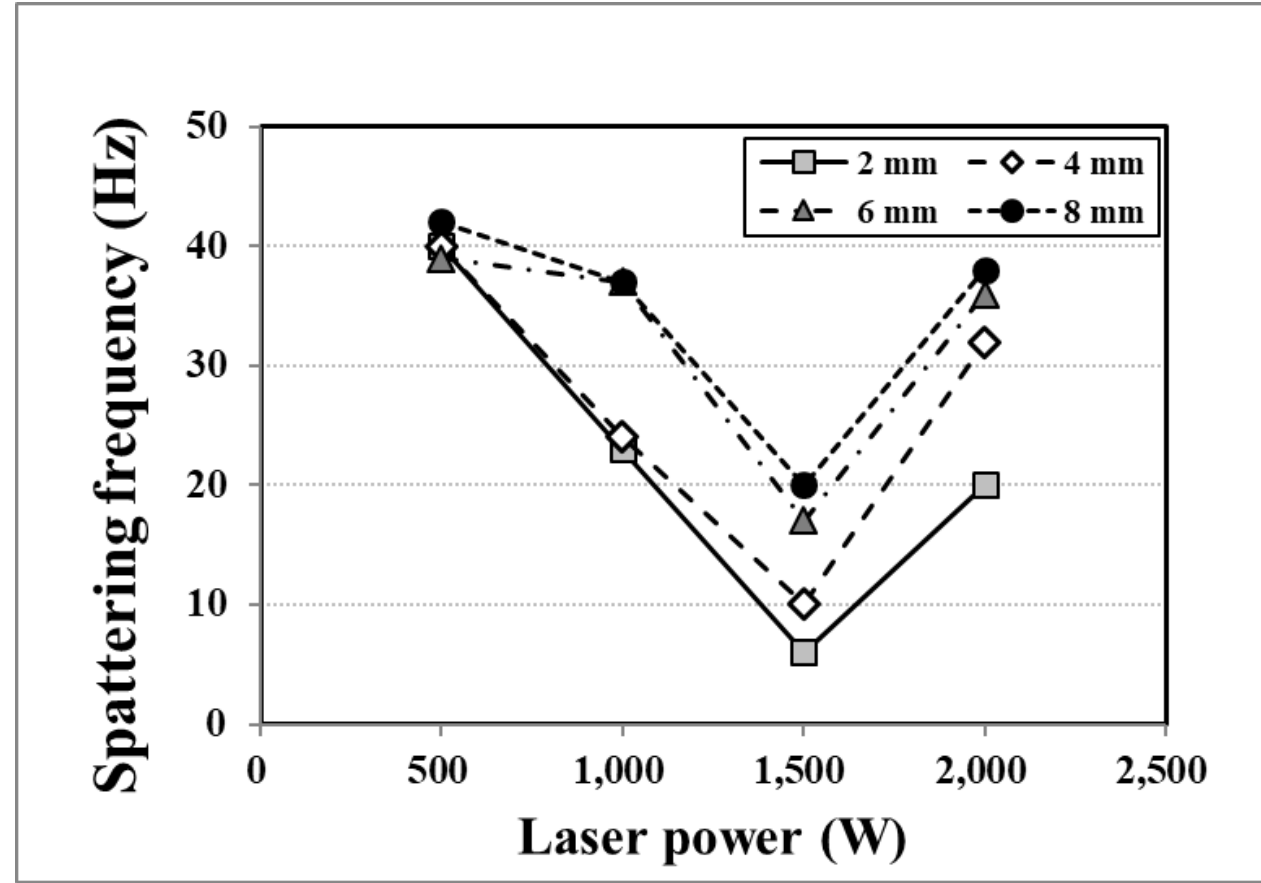


Fig. 11 Effect of laser power on spatter generation. The number of spatters was counted during a 1.0 s interval.

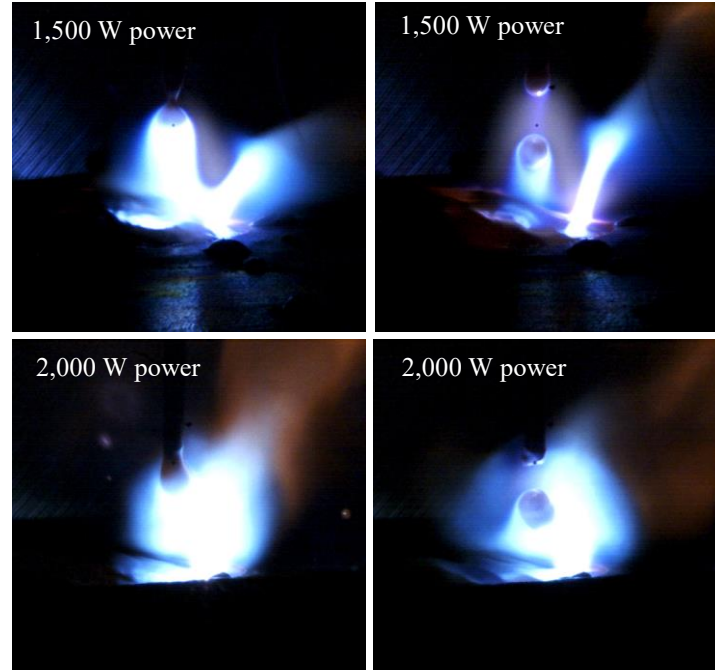


Fig. 12 Cathode jet and plasma behavior according to the laser power at an offset distance of 2 mm

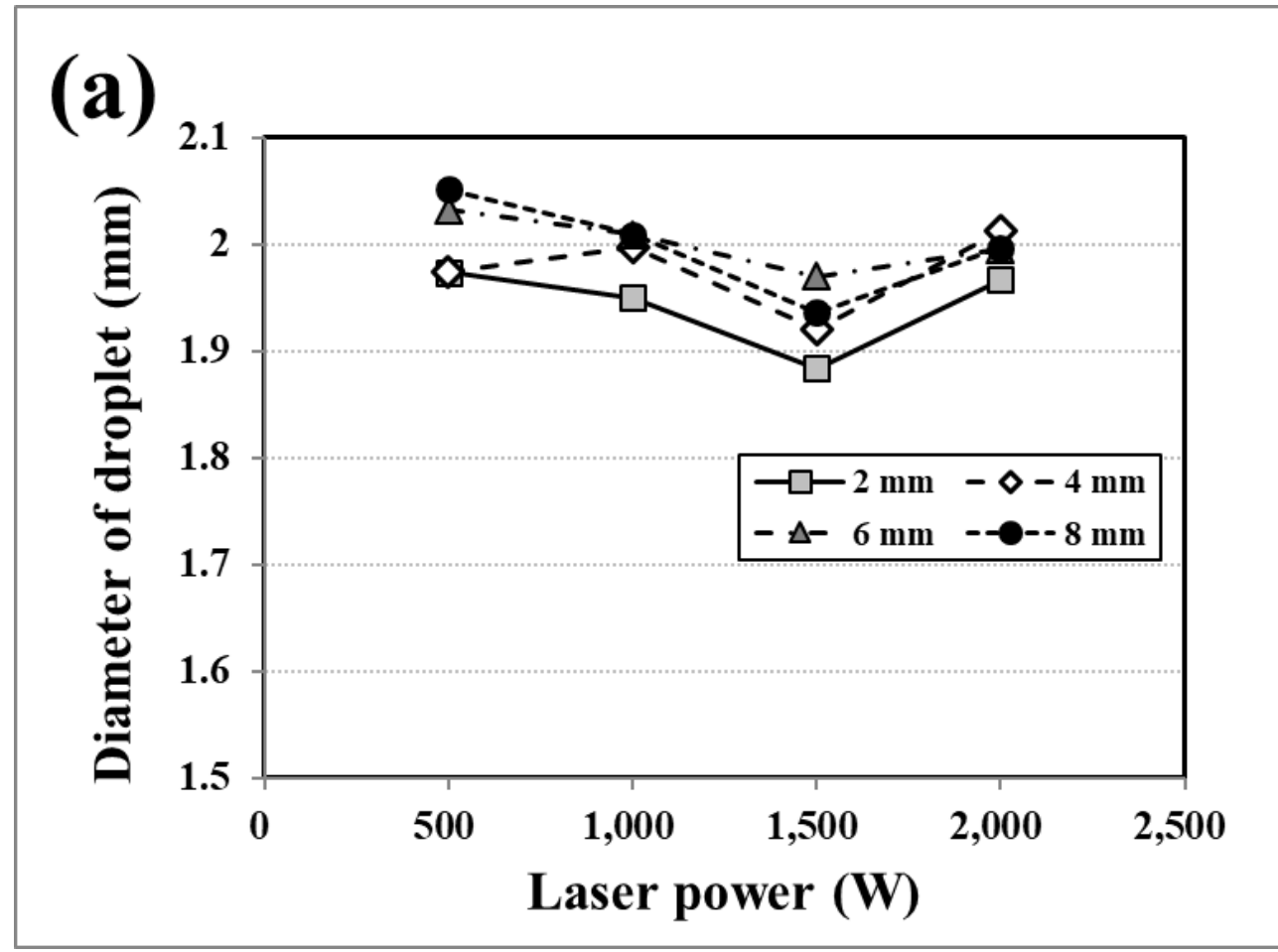


Fig. 13 Measured (a) diameter and (b) frequency of free flight droplet

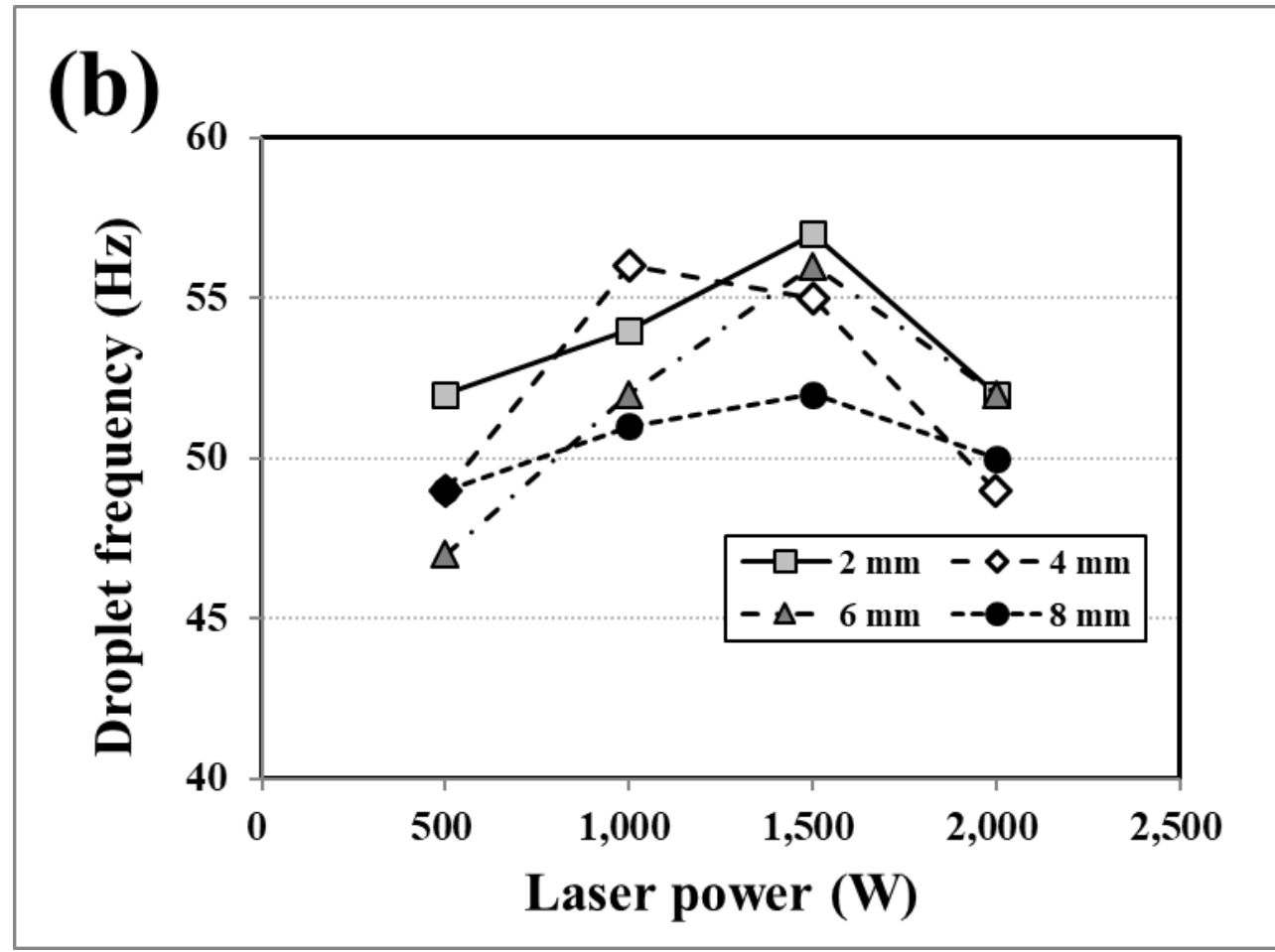


Fig. 13 Measured (a) diameter and (b) frequency of free flight droplet

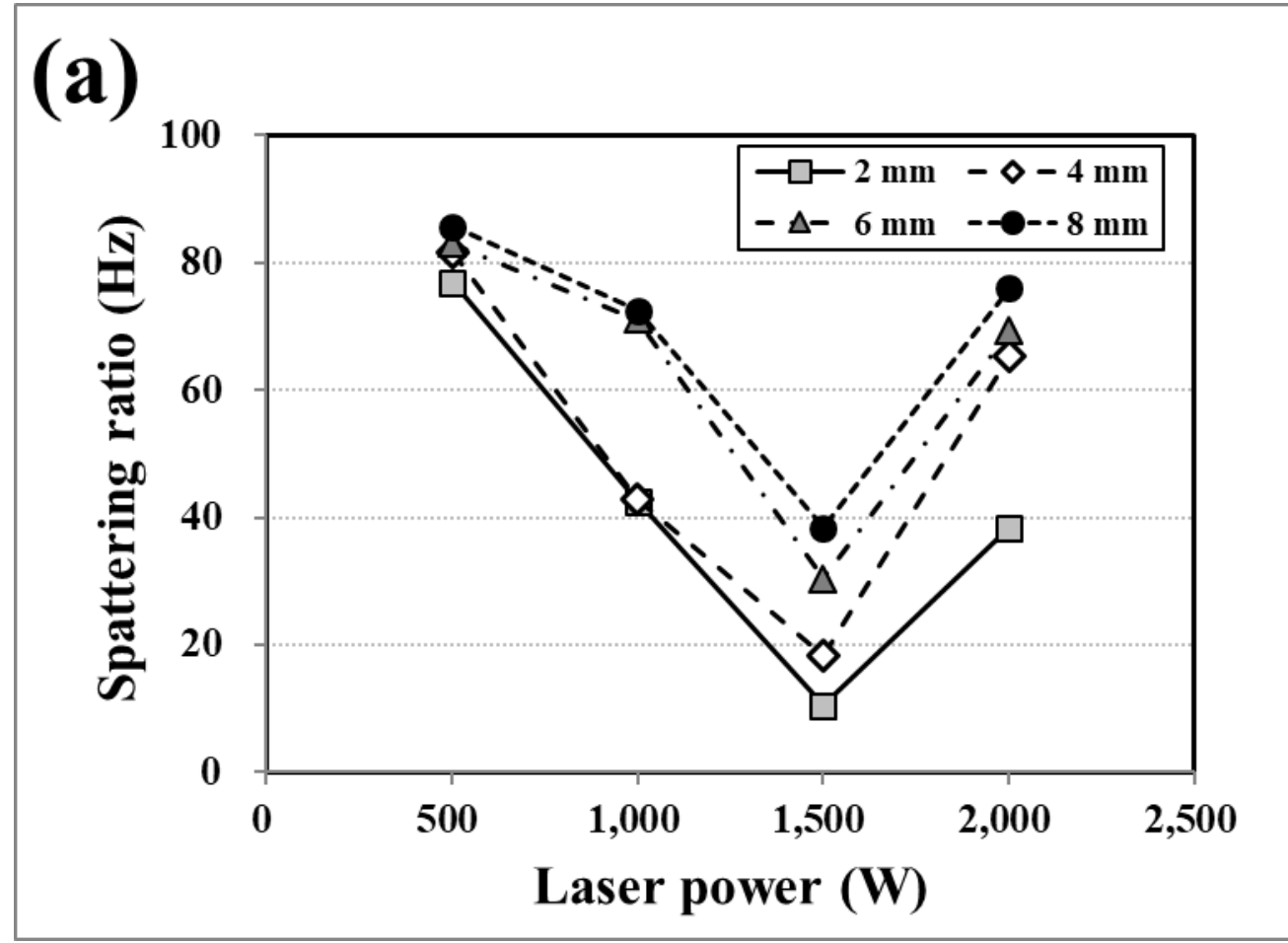


Fig. 14 Calculated (a) spattering ratio and (b) volumetric transfer rate

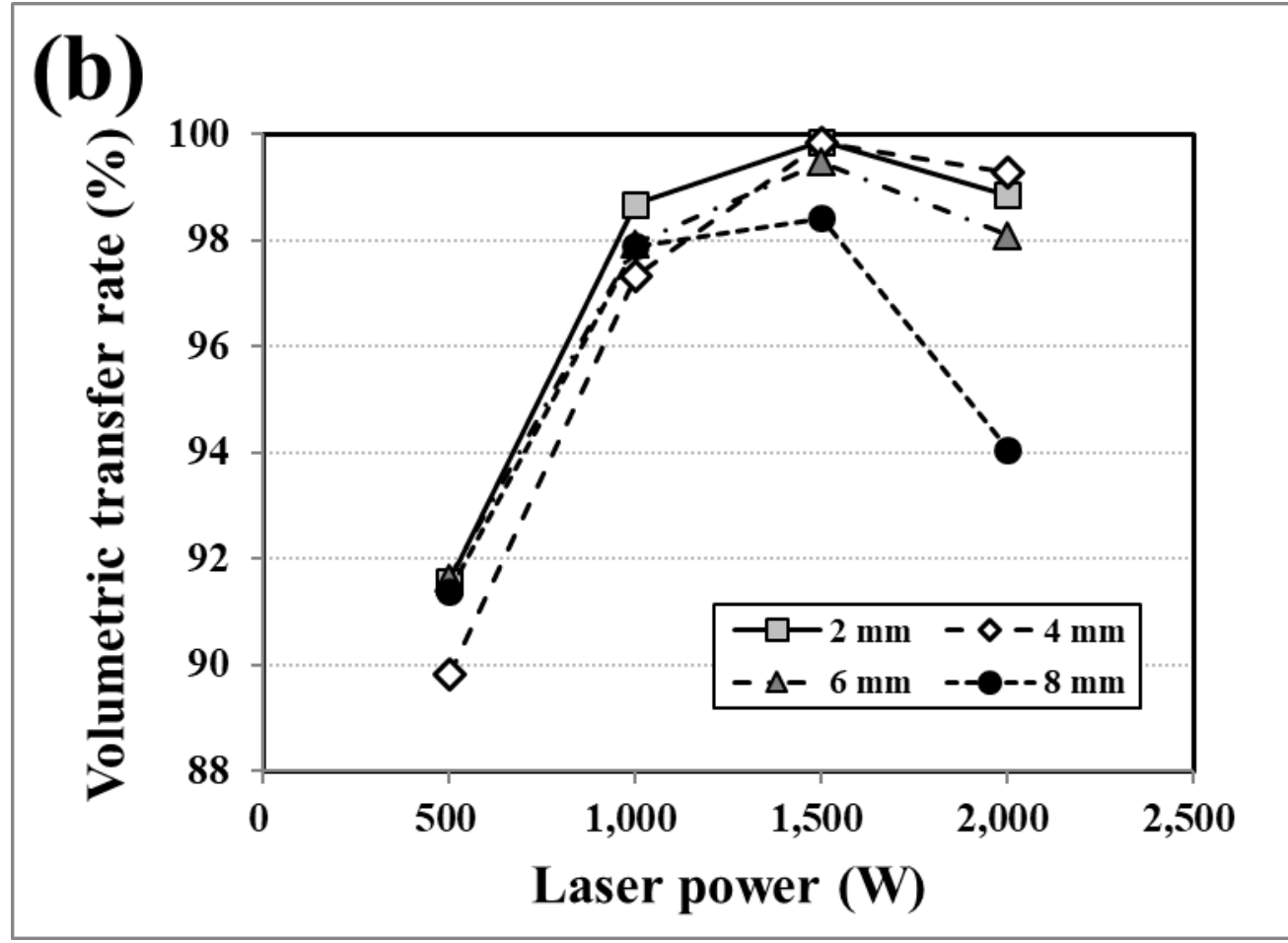


Fig. 14 Calculated (a) spattering ratio and (b) volumetric transfer rate

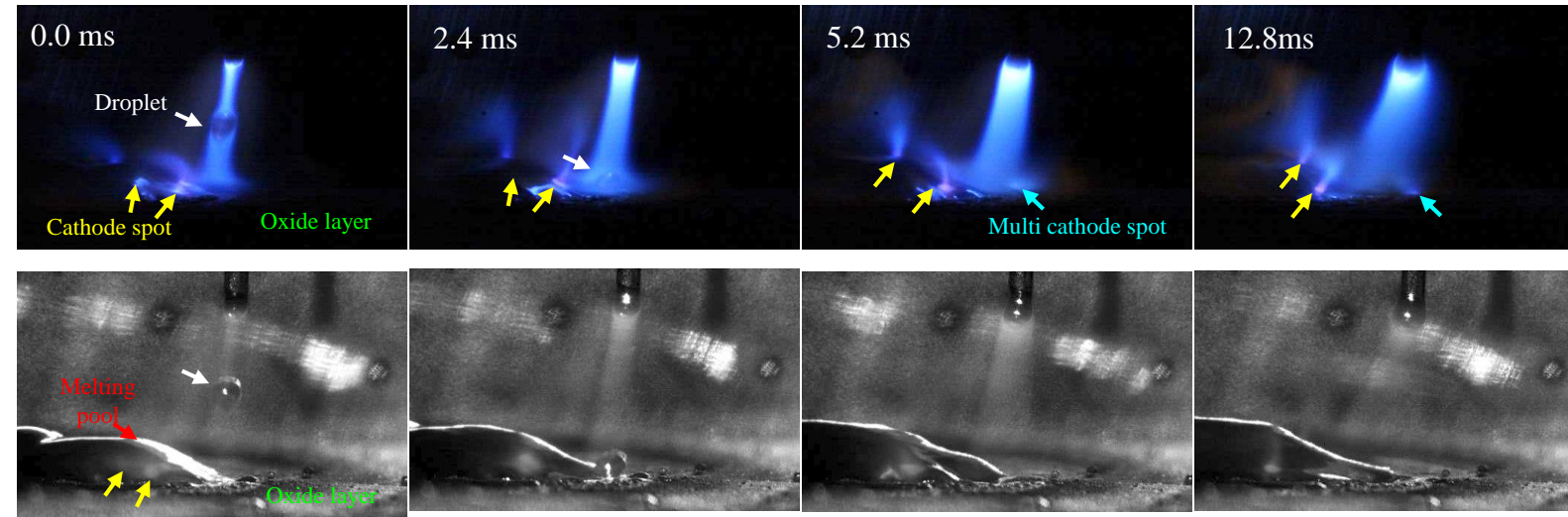


Fig. 15 Cathode spot behavior in oxide-prelaying test

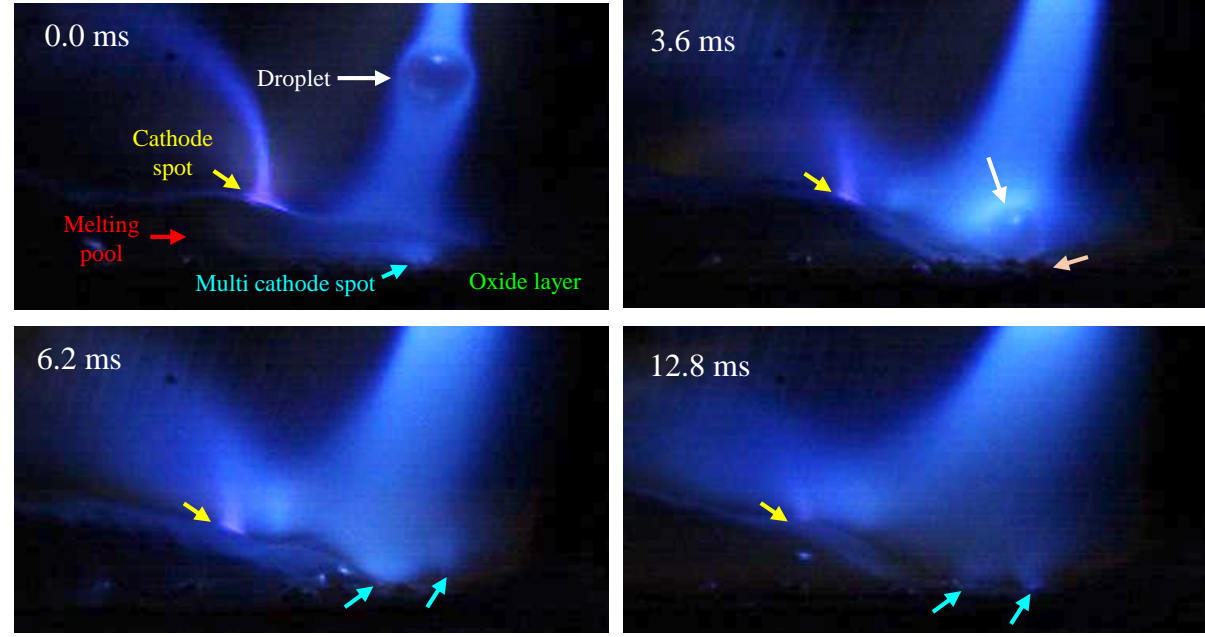


Fig. 16 Multiple cathode spots from oxides

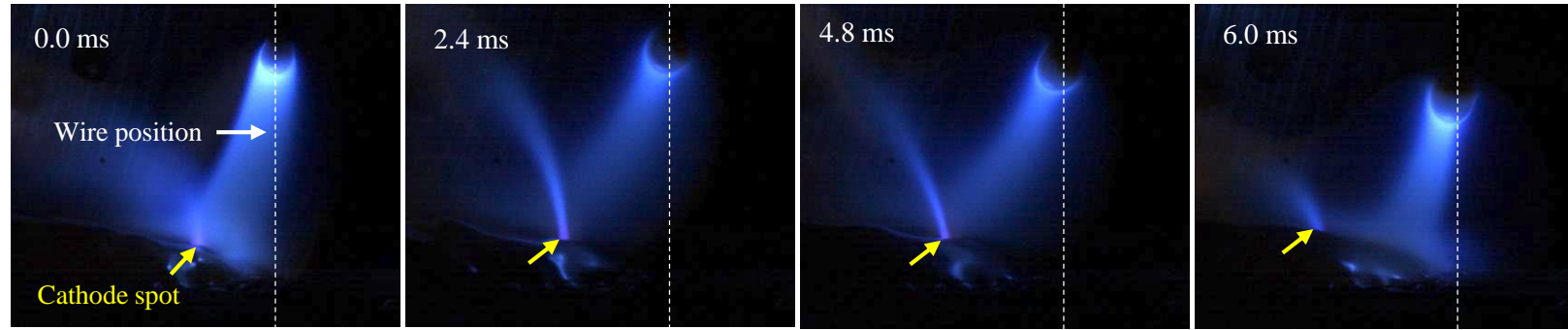


Fig. 17 Arc wandering in the oxide prelaying test